Supplement of 'Results of the second Ice Shelf – Ocean Model Intercomparison Project (ISOMIP+)'

Claire K. Yung[1], Xylar S. Asay-Davis[2], Alistair Adcroft[3], Christopher Y. S. Bull[4], Jan De Rydt[5], Michael S. Dinniman[6], Benjamin K. Galton-Fenzi[7,8], Daniel Goldberg[9], David E. Gwyther[10], Robert Hallberg[3,11], Matthew Harrison[11], Tore Hattermann[12], David M. Holland[13], Denise Holland[13], Paul R. Holland[14], James R. Jordan[15], Nicolas C. Jourdain[16], Kazuya Kusahara[17], Gustavo Marques[18], Pierre Mathiot[16], Dimitris Menemenlis[19], Adele K. Morrison[1], Yoshihiro Nakayama[20,21], Olga Sergienko[3], Robin S. Smith[22], Alon Stern[3], Ralph Timmermann[23], and Qin Zhou[24]

[1]Research School of Earth Sciences and Australian Centre for Excellence in Antarctic Science, The Australian National University, Canberra, Australia
[2]Fluid Dynamics and Solid Mechanics, Los Alamos National Laboratory, Los Alamos, NM 87545, USA
[3]Atmospheric and Oceanic Sciences Program, Princeton University, Princeton, NJ, USA
[4]ACCESS-NRI, Australian National University, Canberra, Australia
[5]Department of Geography and Environmental Sciences, Northumbria University, Newcastle, UK
[6]Center for Coastal Physical Oceanography, Old Dominion University, Norfolk, VA, USA
[7]Australian Antarctic Division, Kingston, Tasmania, Australia
[8]Australian Antarctic Program Partnership (AAPP), Institute for Marine and Antarctic Studies, and the Australian Centre for Excellence in Antarctic Science (ACEAS), both at the University of Tasmania, Australia
[9]School of Geosciences, University of Edinburgh, Edinburgh, UK
[10]School of the Environment, The University of Queensland, St Lucia, QLD, Australia.
[11]NOAA/Geophysical Fluid Dynamics Laboratory, Princeton, NJ, USA
[12]Norwegian Polar Institute, Fram Centre, Tromsø, Norway
[13]Environmental Fluid Dynamics Laboratory, New York University, NY, USA
[14]British Antarctic Survey, Cambridge, UK
[15]Department of Geography, Swansea University, Swansea, UK
[16]Institut des Geosciences de l'Environnement, Univ. Grenoble Alpes/CNRS/IRD/G-INP/INRAE, Grenoble, France
[17]Japan Agency for Marine-Earth Science and Technology (JAMSTEC), Yokohama, Japan
[18]Climate and Global Dynamics Laboratory, National Center for Atmospheric Research, Boulder, CO, USA
[19]Moss Landing Marine Laboratories, Sa José State University, Moss Landing, California, USA
[20]Thayer School of Engineering, Dartmouth College, Hanover, NH, USA
[21]Institute of Low Temperature Science, Hokkaido University, Sapporo, Japan
[22]National Centre for Atmospheric Science, Department of Meteorology, University of Reading, Reading, UK
[23]Alfred-Wegener-Institut für Polar- und Meeresforschung, Bremerhaven, Germany
[24]Akvaplan-niva AS, 9296, Tromsø, Norway

Correspondence: Claire K. Yung (claire.yung@anu.edu.au)

S1 Supplementary Figures

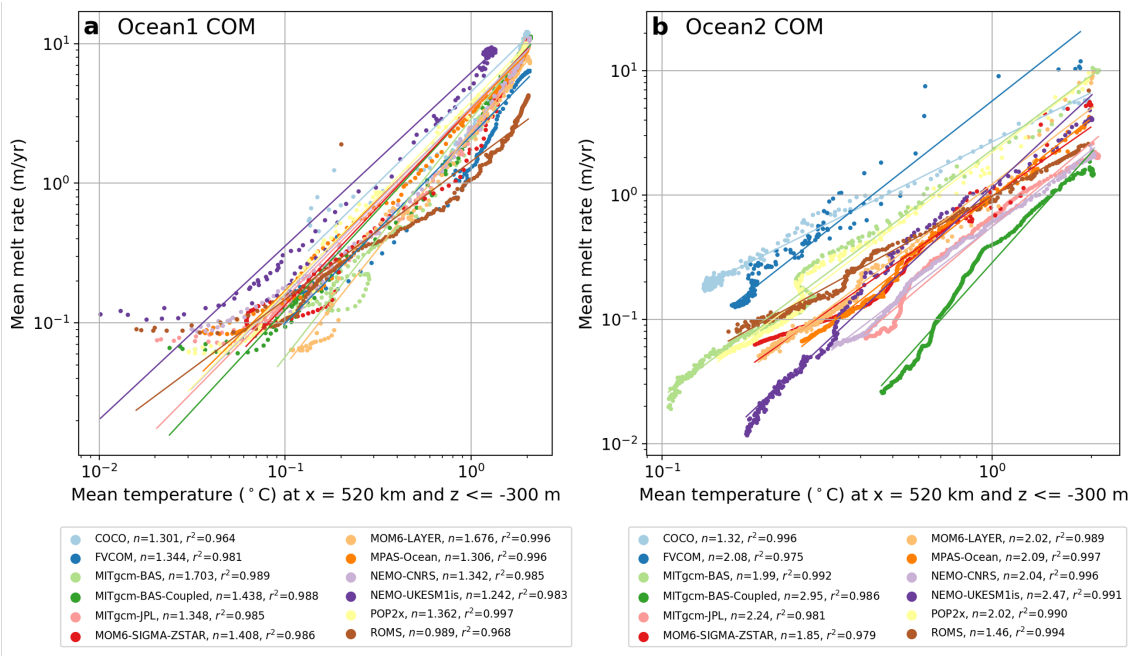

Figure S1. Mean melt rates as a function of ocean temperature (shifted by +2.1°C) at depth, near the ice front. The log-log plot is used to fit $m = T^n$, where n is power law exponent with m the mean melt rate and T the temperature below 300 m at the $x = 520$ km transect. r^2 is the associated Pearson correlation coefficient. Panel a shows Ocean1 COM and b shows Ocean2 COM. Pearson correlation coefficients are high, with power-law exponents averaging 1.3 for Ocean1 and 2 for Ocean2.

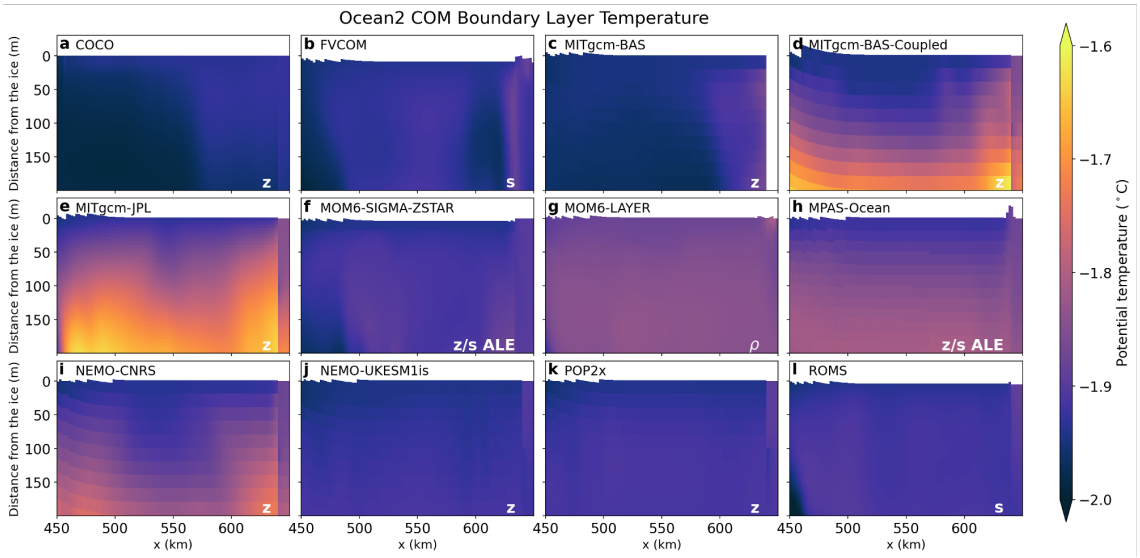

Figure S2. Boundary Layer Temperature, Ocean2 COM, averaged over year 20 as in Fig. 13.

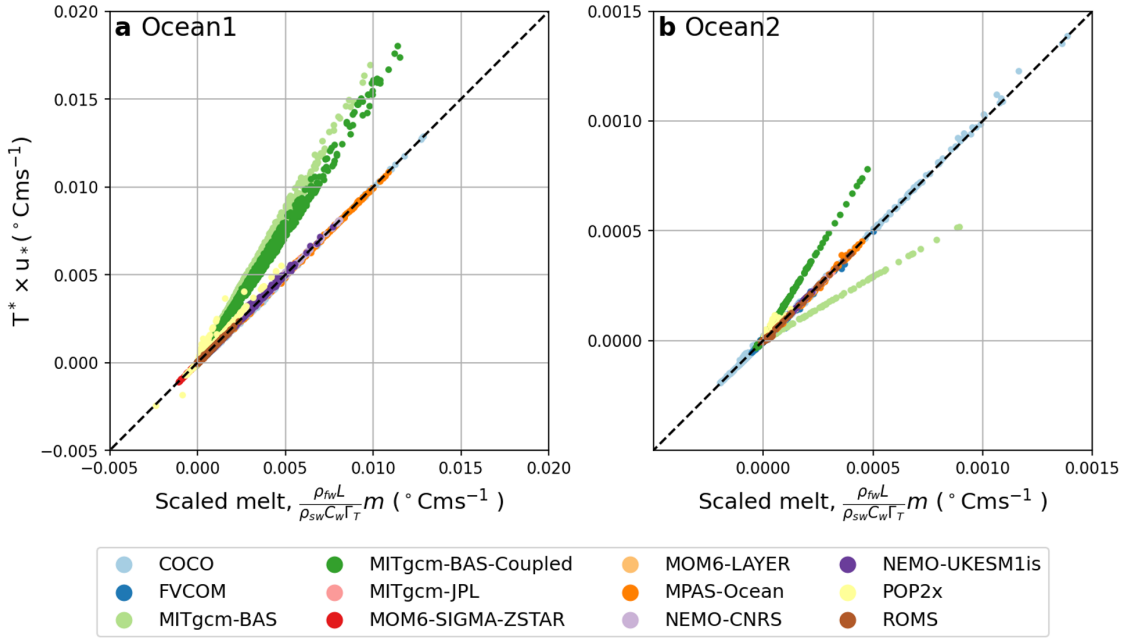

Figure S3. Thermal driving multiplied by friction velocity, averaged over year 20 for each model, against melt rate scaled by constants in Eqn. 1b (Table 2). Panel a shows Ocean1 COM results and Panel b shows Ocean2 COM. For MITgcm-BAS, the Ocean1 value in Table 2 is used in both panels.

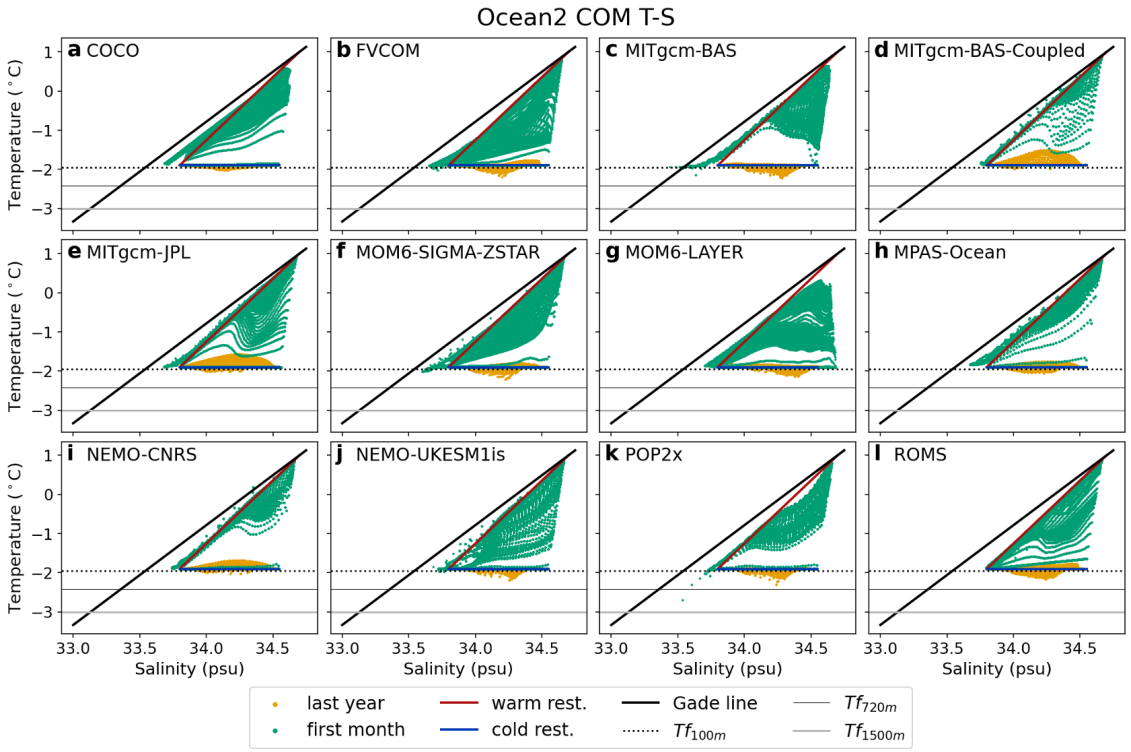

Figure S4. Temperature-Salinity space verification for Ocean2 COM, as in Fig. 15.

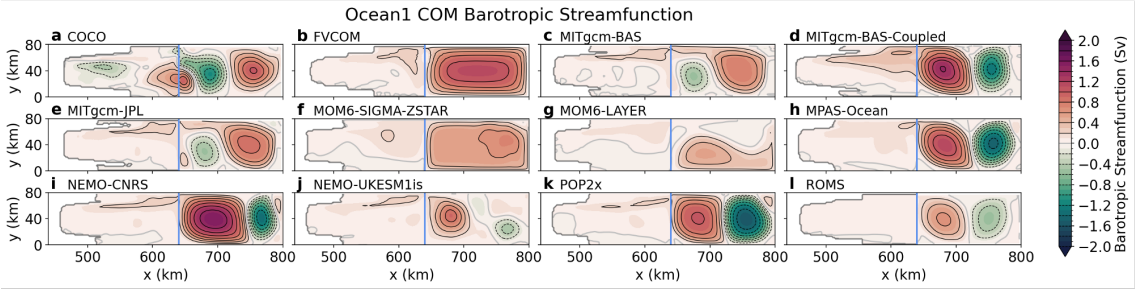

Figure S5. Ocean1 COM barotropic streamfunction averaged over year 20, corresponding to the steady warm state of the cavity, for the full domain.

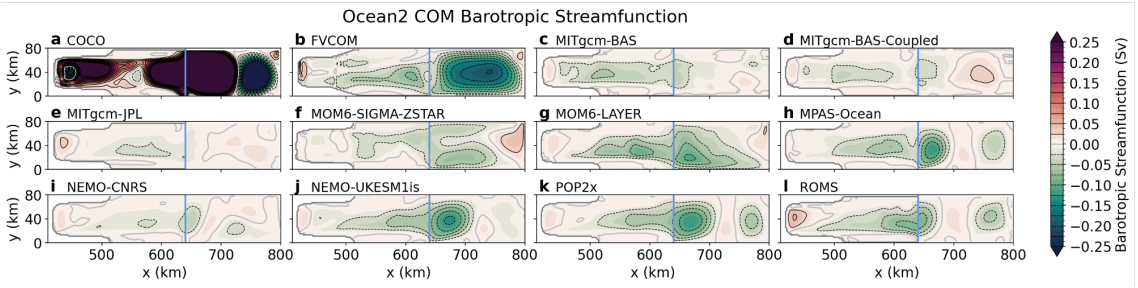

Figure S6. Ocean 2 COM barotropic streamfunction averaged over year 20, corresponding to the steady cold state of the cavity, for the full domain.

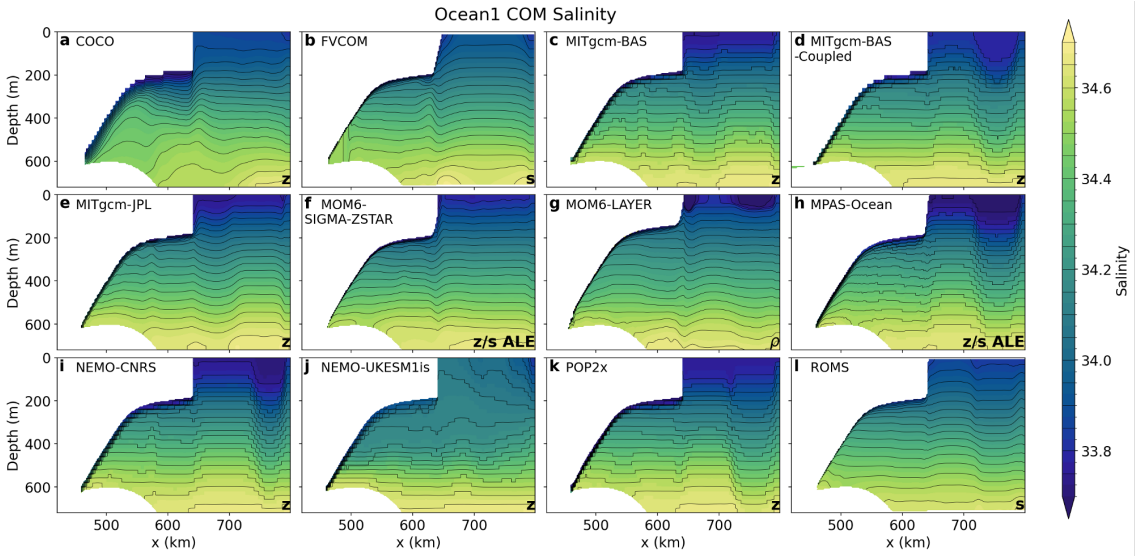

Figure S7. Salinity transect of Ocean1 COM through y = 40 km, averaged over year 20.

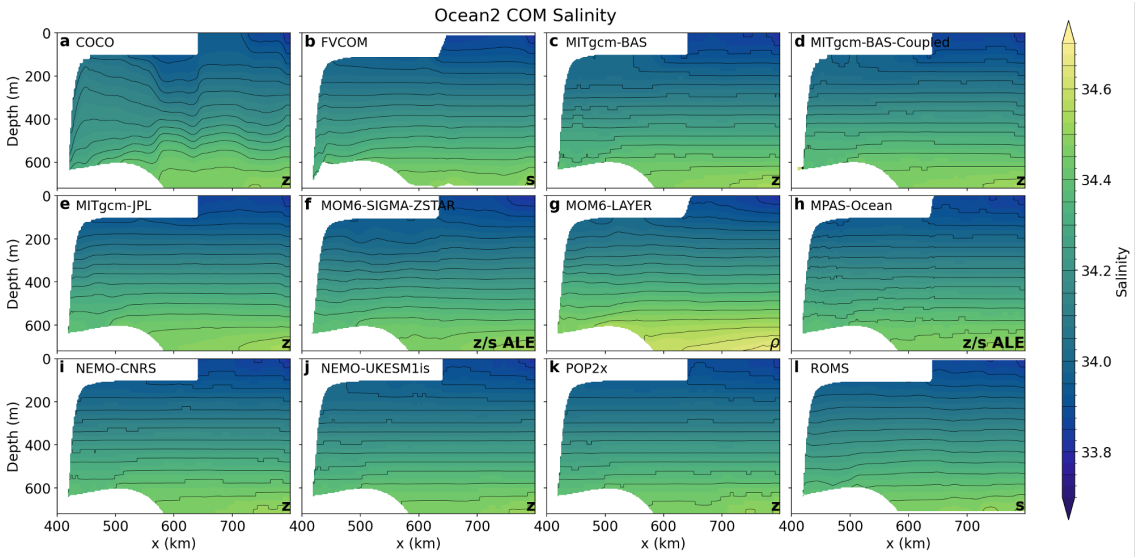

Figure S8. Salinity transect for Ocean2 COM through y = 40 km, averaged over year 20.

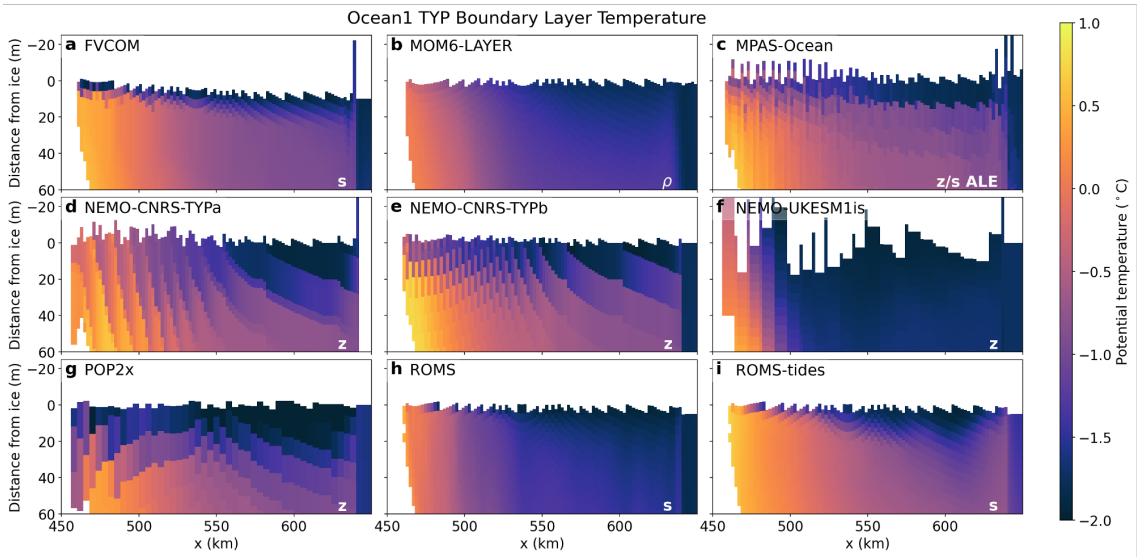

Figure S9. Boundary layer temperature, for Ocean1 TYP, averaged over year 20 as in Fig. 13.

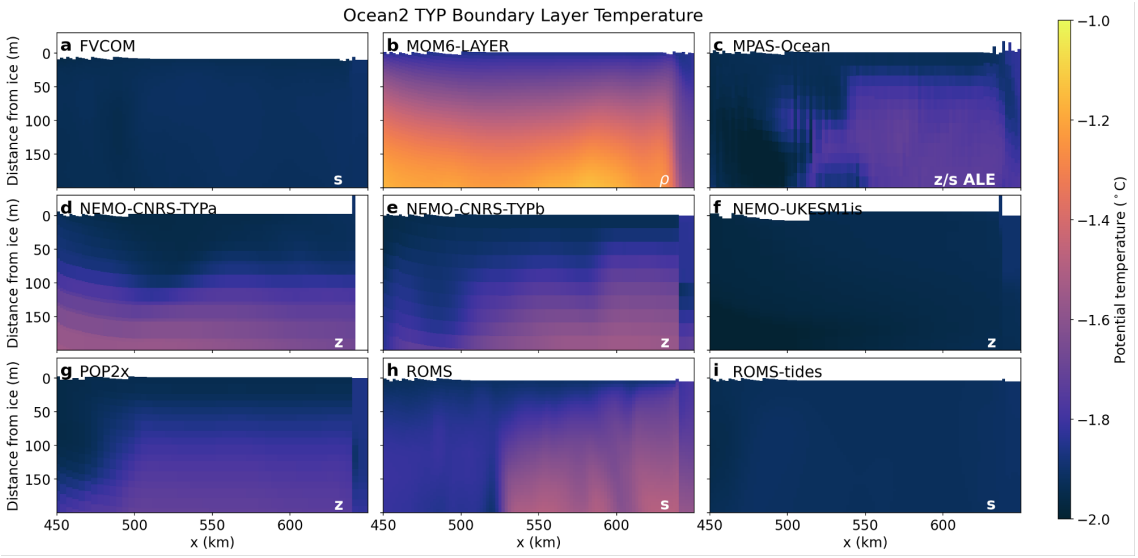

Figure S10. Boundary layer temperature, for Ocean2 TYP, averaged over year 20 as in Fig. 13.

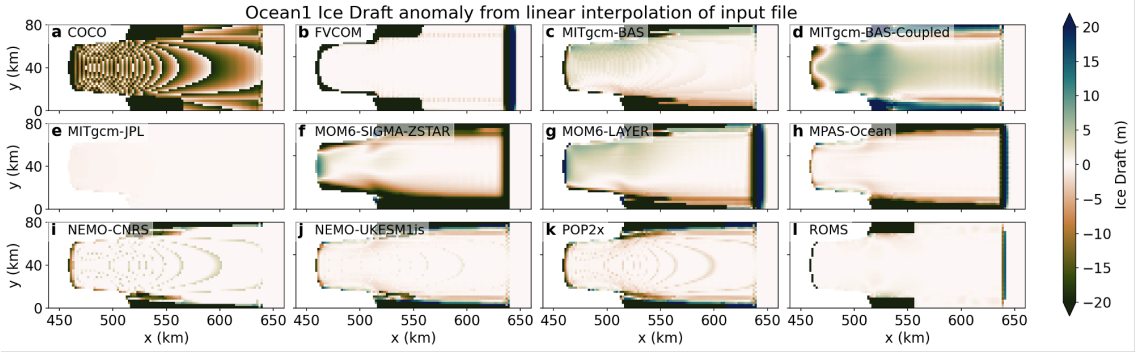

Figure S11. Ocean1 ice draft (position of ice-ocean interface) anomaly from linear interpolation of provided input file. Positive values have a thicker ice draft.

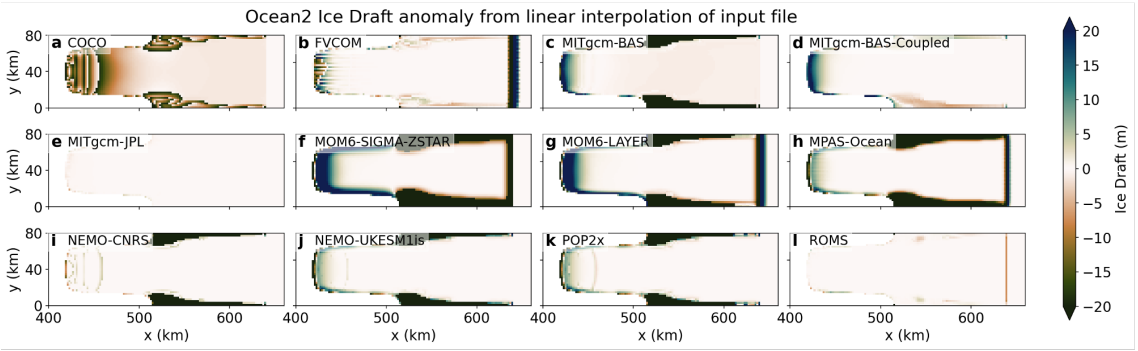

Figure S12. Ocean2 ice draft (position of ice-ocean interface) anomaly from linear interpolation of provided input file. Positive values have a thicker ice draft.

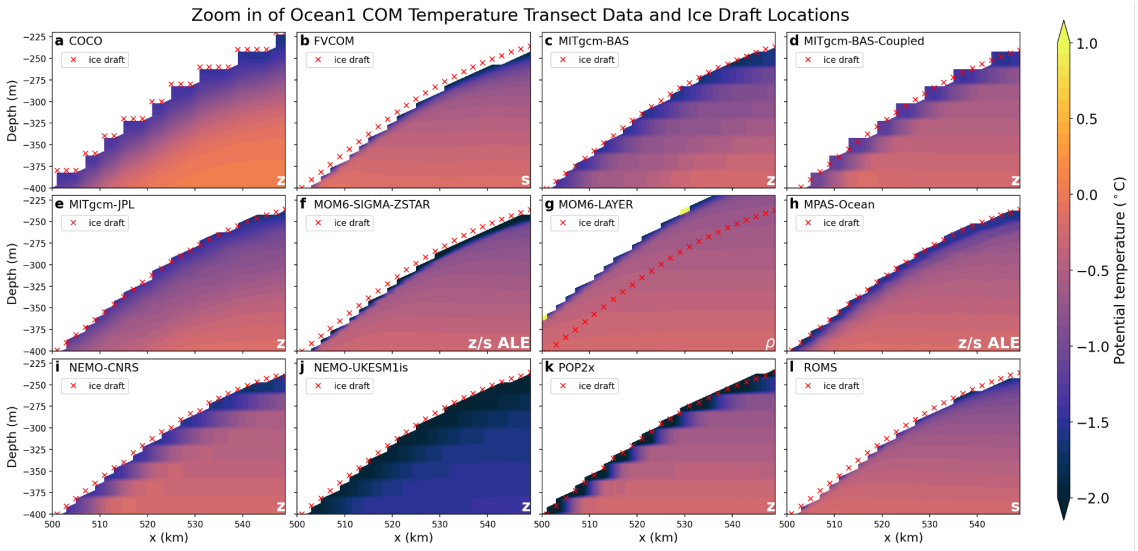

Figure S13. Temperature along the $y = 40$ km transect at year 20, zoomed into the region x =500-550 km, to demonstrate the 'distance from the ice' plotting of Fig. 13. Red crosses indicate the ice draft output and colours indicate the temperature data output, which is in 5 m depth discretisation. Modelling groups remapped their data from the model's native grid to the native grid in different ways. Sea level rise is seen in MOM6-LAYER as the ice draft is from time zero; a correction is employed in Fig. 13 to shift the ice draft to the appropriate depth.

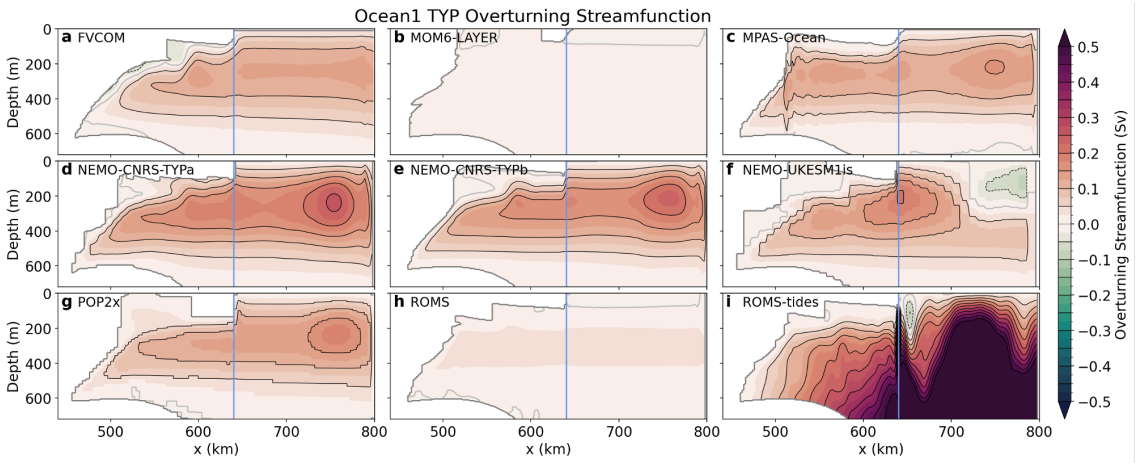

Figure S14. Overturning streamfunction averaged over year 20 of the Ocean1 TYP experiment.

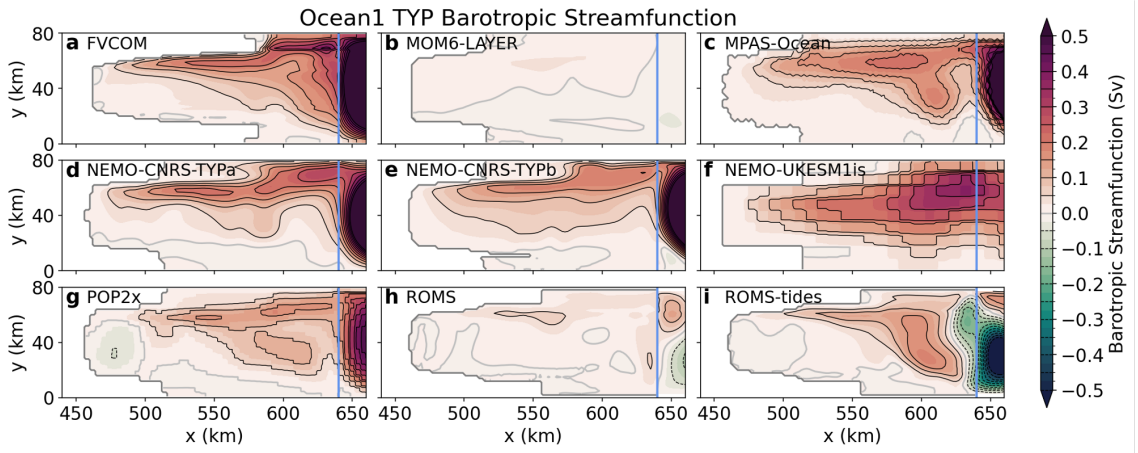

Figure S15. Barotropic streamfunction averaged over year 20 of the Ocean1 TYP experiment, focusing on the ice shelf cavity.